⌘ *Author's Choice*

THE JOURNAL OF BIOLOGICAL CHEMISTRY VOL. 286, NO. 1, pp. 674–686, January 7, 2011

Proteomic Analysis of Native Hepatocyte Nuclear Factor-4α (HNF4α) Isoforms, Phosphorylation Status, and Interactive Cofactors*[S]

Received for publication, June 15, 2010, and in revised form, November 1, 2010 Published, JBC Papers in Press, November 3, 2010, DOI 10.1074/jbc.M110.154732

Kenji Daigo[‡1], Takeshi Kawamura[‡1], Yoshihiro Ohta[‡1], Riuko Ohashi[§], Satoshi Katayose[¶], Toshiya Tanaka[‡], Hiroyuki Aburatani[‡], Makoto Naito[§], Tatsuhiko Kodama[‡], Sigeo Ihara[‡], and Takao Hamakubo[‡2]

From the [‡]Research Center for Advanced Science and Technology, University of Tokyo, Tokyo 153-8904, the [§]Division of Cellular and Molecular Pathology, Niigata University Graduate School of Medical and Dental Sciences, Niigata 951-8510, and the [¶]Tsukuba Research Laboratories, JSR Corporation, Ibaraki 305-0841, Japan

Hepatocyte nuclear factor-4α (HNF4α, NR2A1) is a nuclear receptor that has a critical role in hepatocyte differentiation and the maintenance of homeostasis in the adult liver. However, a detailed understanding of native HNF4α in the steady-state remains to be elucidated. Here we report the native HNF4α isoform, phosphorylation status, and complexes in the steady-state, as shown by shotgun proteomics in HepG2 hepatocarcinoma cells. Shotgun proteomic analysis revealed the complexity of native HNF4α, including multiple phosphorylation sites and inter-isoform heterodimerization. The associating complexes identified by label-free semiquantitative proteomic analysis include the following: the DNA-dependent protein kinase catalytic subunit, histone acetyltransferase complexes, mRNA splicing complex, other nuclear receptor coactivator complexes, the chromatin remodeling complex, and the nucleosome remodeling and histone deacetylation complex. Among the associating proteins, GRB10 interacting GYF protein 2 (GIGYF2, PERQ2) is a new candidate cofactor in metabolic regulation. Moreover, an unexpected heterodimerization of HNF4α and hepatocyte nuclear factor-4γ was found. A biochemical and genomewide analysis of transcriptional regulation showed that this heterodimerization activates gene transcription. The genes thus transcribed include the cell death-inducing DEF45-like effector b (*CIDEB*) gene, which is an important regulator of lipid metabolism in the liver. This suggests that the analysis of the distinctive stoichiometric balance of native HNF4α and its cofactor complexes described here are important for an accurate understanding of transcriptional regulation.

Hepatocyte nuclear factor-4α (HNF4α)[3] is an orphan nuclear receptor (NR), which plays a critical role in hepatocyte differentiation (1–3) as well as the maintenance of homeostasis of the adult liver, intestine, and pancreatic β cells (4–7). Human HNF4α gene mutations cause maturity onset diabetes of the young 1 (MODY1) (8, 9), and the HNF4α ligands have been extended to include fatty acid metabolites (10–12). HNF4α consists of six distinct functional domains (A to F) (13), an A/B domain, which is associated with activation function 1 (AF-1), a C domain, which binds certain specific DNA sequences, a 6-base pair repeat segment with a 1-base pair spacer called direct repeat 1 (DR1), an E domain, which is the homodimerization region and also the ligand-binding domain associated with activation function 2, and an F domain, which has a negative regulatory function. Odom *et al.* (14) used a systemic promoter microarray analysis of HNF4α to reveal that the majority of active RNA polymerase II binding genes were also occupied by HNF4α in human hepatocytes, and concluded that the major function of HNF4α in the adult liver is the constitutive regulation of diverse genes.

The key factors in the wide diversity of the HNF4α-regulated transcriptional machinery are the phosphorylation and isoform states along with cofactor interactions. The phosphorylation of HNF4α regulates specific genes by affecting DNA binding and/or cofactor recruitment (15–18). The HNF4α isoforms are generated by alternative promoters together with alternative splicing of the corresponding exons (19–21). Although partially redundant, specific isoforms modulate transcriptional activity, cofactor recruitment, and specific gene regulation (22–25). Certain HNF4α-interacting cofactors alter HNF4α-regulated transcriptional mechanisms (15, 23, 24). In the commonly postulated NR mechanism, ligand binding induces the replacement of a histone deacetylase complex with a histone acetyltransferase (HAT) complex, with binding taking place through the NR-coregulator interaction motifs together with the activation function 2 domain

* This work was supported by the Program for Promotion of Fundamental Studies in Health Sciences of the National Institute of Biomedical Innovation (NIBIO), Japan, Development of New Functional Antibody Technologies of the New Energy and Industrial Technology Development Organization (NEDO), Japan, and Japan Grants-in-Aid for Scientific Research 19319129, 19800009, and 20221010 from the Ministry of Education, Culture, Sports, Science and Technology.

⌘ *Author's Choice*—Final version full access.

[S] The on-line version of this article (available at http://www.jbc.org) contains supplemental Figs. S1–S3, Table S1, and Data S1 and S2.

[1] These authors contributed equally to this work.

[2] To whom correspondence should be addressed: Research Center for Advanced Science and Technology, The University of Tokyo, 4-6-1 Komaba, Meguro, Tokyo 153-8904, Japan. Tel./Fax: 81-3-5452-5231; E-mail: hamakubo@lsbm.org.

[3] The abbreviations used are: HNF4α, hepatocyte nuclear factor-4α; ChIP-seq, chromatin immunoprecipitation sequencing; CIDEB, cell death-inducing DFFA-like effector b; DNA-PKcs, DNA-dependent protein kinase catalytic subunit; DR1, direct repeat 1; HAT, histone acetyltransferase; HGD, homogentisate 1,2-dioxygenase; HNF4γ, hepatocyte nuclear factor-4γ; IP, immunoprecipitation; NR, nuclear receptor; STAGA, SPT3-TAF$_{II}$31-GCN5L acetylase; HPRD, Human Protein Reference Database.

(26). Recent reports showed that the cofactor-mediated function results in histone modification, regulation of chromatin conformation, and immature mRNA metabolism (27). Whereas these key factors might be linked with each other and have a central role in the fine tuning of the multiple transcriptional regulation activities performed by HNF4α, the details of the steady-state of native HNF4α are, as yet, poorly understood.

Hepatocyte nuclear factor-4γ (HNF4γ, NR2A2) is a member of the HNF4 orphan subfamily expressed in the pancreas, kidney, small intestine, and testis (28). Whereas an early report suggested there was no expression in the human liver (28), other groups subsequently reported expression at the mRNA level (29, 30). The gene regulation effected by HNF4γ has been reported to take place in coordination with HNF4α (31–33). In the study of Bogan *et al.* (34), they predicted the heterodimerization of HNF4α and HNF4γ through $K(X)_{26}E$ motifs on the E domain.

Here, we investigated the steady-state native HNF4α isoform, as well as the phosphorylation state and interacting complex, by shotgun proteomics and label-free semiquantitative proteomic analysis using specific antibodies and low noise magnetic beads. Moreover, by utilizing the complex database, we were able to categorize the cofactors into functional complexes. The data indicate the complexity of the native HNF4α states and cofactors obtained via stoichiometry. In confirmation of this proteomic analysis, we unexpectedly demonstrated HNF4α and HNF4γ heterodimerization and transcriptional activation. The regulatory genes shown here include an important regulator of lipid metabolism in the liver. The results support the concept that the fine tuning of the multiple transcriptional regulation activities arose from a distinctive stoichiometric balancing of the nuclear receptor and interacting cofactors. The application of this method to dynamic proteomics should help provide a means to obtain an adequate understanding of transcriptional regulation in extracellular/intracellular signaling and/or the developmental cascade.

EXPERIMENTAL PROCEDURES

Antibodies—Mouse monoclonal antibody H1415 (IgG2a) directed against the F domain, K9218 (IgG2a) directed against the P1-driven A/B domain, H6939 (IgG1) directed against the P2-driven A/B domain of human HNF4α, and B6502A (IgG1) directed against human HNF4γ, were raised in our laboratory by immunizing separate mice with peptides representing residues 394 to 461 of human HNF4α isoform 2, 3 to 49 of human HNF4α isoform 2, 1 to 16 of human HNF4α isoform 7, and 91 to 212 of human HNF4γ, respectively.

Preparation of Monoclonal Antibody Cross-linked Protein G-conjugated Magnetic Beads—Magnetic beads with Protein G conjugated on their surface (Magnosphere™ MS300/Protein G, JSR Corp., Japan) were washed twice with PBS, 0.05% Tween 20. The capturing antibody procedure was carried out by adding the antibody at a final ratio of 4 μg of antibody/1 mg of beads with gentle mixing for 40 min at room temperature. After washing twice with PBS, 0.05% Tween 20 followed by 0.2 M triethanolamine-HCl, pH 8.2, the affinity-captured antibody was cross-linked by adding 20 mM dimethyl pimelimidate in 0.2 M triethanolamine-HCl, pH 8.2, with gentle mixing for 30 min at room temperature. After removing the buffer, quenching was carried out by adding Tris-buffered saline with gentle mixing for 15 min at room temperature. After washing twice with PBS, 0.01% Tween 20, antibody cross-linked Protein G-conjugated magnetic beads were suspended with PBS, 0.01% Tween 20 and stored at 4 °C.

Preparation of HepG2 Nuclear Extract—HepG2 cells were grown as previously described (35). HepG2 nuclear extract was prepared described by Dignam *et al.* (36), with minor changes. All steps were carried out at 4 °C. The culture medium was removed from HepG2 cell cultures grown to 80–90% confluence. The cells were gently rinsed with ice-cold PBS, 0.2 mM PMSF and harvested by scraping into fresh ice-cold PBS, 0.2 mM PMSF. Harvested cells were collected by centrifugation for 10 min at 1,850 × *g* and resuspended in a 5 packed cell volume of hypotonic buffer (10 mM HEPES, pH 7.9, at 4 °C, 1.5 mM $MgCl_2$, 10 mM KCl, 0.2 mM PMSF, 0.5 mM DTT). Suspension cells were again collected by centrifugation for 5 min at 1,850 × *g* and resuspended in hypotonic buffer to a final volume of 3 packed cell volume. The cells were transferred to a glass Dounce homogenizer after incubating on ice for 10 min and homogenized using a loose pestle with 25 to 30 gentle strokes. When cell lysis reached 80%, the nuclei were collected by centrifugation for 15 min at 3,300 × *g*. The nuclei pellet was resuspended in 1/2 packed nuclear volume of low-salt buffer (20 mM HEPES, pH 7.9, at 4 °C, 25% glycerol, 1.5 mM $MgCl_2$, 20 mM KCl, 0.2 mM EDTA, 0.2 mM PMSF, 0.5 mM DTT). In terms of the nuclear extract preparation, 1/2 packed nuclear volume of high-salt buffer (20 mM HEPES, pH 7.9, at 4 °C, 25% glycerol, 1.2 M $MgCl_2$, 20 mM KCl, 0.2 mM EDTA, 0.2 mM PMSF, 0.5 mM DTT) was added to the nuclei suspension in a dropwise fashion over a period of 1 h with gentle stirring, and then continuously stirred gently for 30 min at 4 °C. The extract was centrifuged 30 min at 25,000 × *g* to remove debris, and the supernatant was dialyzed against a sufficient volume of dialysis buffer (20 mM HEPES, pH 7.9, at 4 °C, 10% glycerol, 100 mM KCl, 0.2 mM EDTA, 0.2 mM PMSF) for 5 h. The dialyzed extract was centrifuged for 20 min at 25,000 × *g*, and the pellet was discarded. Aliquots of the supernatant were frozen with liquid nitrogen and stored at −80 °C as the nuclear extract.

Immunoprecipitation of Native HNF4α Complex from HepG2 Nuclear Extract—Before affinity purification, the HepG2 nuclear extract was thawed on ice, added at the final concentration of 0.1% Nonidet P-40, centrifuged 15 min at 20,000 × *g*, and the pellet was discarded. Supernatant was passed through a 0.22-μm filter and incubated with 0.5 mg of the antibody cross-linked Protein G-conjugated magnetic beads for 4 h at 4 °C. Magnet beads were washed 3 times with 0.1 M KCl-HEGN (20 mM HEPES, pH 7.9, at 4 °C, 0.1 M KCl, 0.1 mM EDTA, 10% glycerol, 0.1% Nonidet P-40, 0.2 mM PMSF) and once with 50 mM NH_4HCO_3 buffer at 4 °C. The affinity purified proteins were eluted by 0.05% RapiGest (Waters) in 50 mM NH_4HCO_3 buffer for 30 min at 67 °C. Eluent was concentrated by 10% ice-cold TCA, washed with ice-cold acetone, and dried. All magnetic bead operations for affinity

purification were carried out with a Magnatrix 1200 (Precision System Science) magnetic bead reaction system.

In-solution Digestion—The immunoprecipitation (IP) samples concentrated by TCA precipitation were resuspended in 25% (v/v) CH_3CN, 25 mM NH_4HCO_3 buffer. The samples were reduced in 1.2 mM tris(2-carboxyethyl)phosphine for 15 min at 50 °C and alkylated in 3 mM iodoacetamide for 30 min at room temperature, respectively. The samples were digested overnight with 100 ng of trypsin (Promega) at 37 °C. After drying with a SpeedVac (ThermoFisher Scientific) to reduce the CH_3CN concentration, peptides were dissolved in 0.2% TFA, 2% CH_3CN solution and incubated for 60 min at 37 °C for residual RapiGest degradation. After incubation, samples were centrifuged to remove precipitates.

Liquid Chromatography-Tandem Mass Spectrometry (LC/MS/MS)—A capillary reverse phase HPLC-MS/MS system (ZAPLOUS System; AMR Inc.), comprised of a Paradigm MS4 quadra solvent delivery device (Michrom BioResources), an HTC PAL autosampler (CTC Analytics), and Finnigan LTQ orbitrap XL mass spectrometer (Thermo Scientific) equipped with an XYZ nanoelectrospray ionization source (AMR Inc.), was used for LC/MS/MS analysis. Aliquots of trypsinized samples were automatically injected onto a peptide CapTrap cartridge (2.0 × 0.5 mm inner diameter, Michrom BioResources) attached to an injector valve for desalting and concentrating the peptides. After washing the trap with 98% H_2O, 2% AcCN, 0.2% TFA, the peptides were loaded into a separation capillary reverse phase column (Monocap C18 150 × 0.2 mm inner diameter, GL-Science) by switching the valve. The eluents used were: A, 98% H_2O, 2% AcCN, 0.1% HCOOH; and B, 10% H_2O, 90% AcCN, 0.1% HCOOH. The column was developed at the flow rate of 1.0 μl/min, with a concentration gradient of AcCN: from 5% B to 35% B for 100 min, then from 35% B to 95% B for 1 min, maintained in 95% B for 9 min, from 95% B to 5% B for 1 min, and finally re-equilibrating with 5% B for 9 min. Effluents were introduced into the mass spectrometer via the nanoelectrospray ion interface that held the separation column outlet directly connected with an nanoelectrospray ionization needle (PicoTip FS360–50-30; New Objective Inc.). The ESI voltage was 2.0 kV and the transfer capillary of the LTQ inlet was heated to 200 °C. No sheath or auxiliary gas was used. The mass spectrometer was operated in a data-dependent acquisition mode, in which the MS acquisition with a mass range of m/z 420–1600 was automatically switched to MS/MS acquisition under the automated control of Xcalibur software. The top 4 precursor ions were selected by an MS scan, with Orbitrap at a resolution of $r = 60000$, and for the subsequent MS/MS scans by ion trap in the normal/centroid mode, using the automated gain control (AGC) mode with AGC values of 5.00×10^5 and 1.00×10^4 for full MS and MS/MS, respectively. We also employed a dynamic exclusion capability that allowed sequential acquisition of the MS/MS of abundant ions in the order of their intensities with an exclusion duration of 2.0 min, and exclusion mass widths of −5 and +5 ppm. The trapping time was 100 ms with the auto gain control on.

Data Base Search and Label-free Semiquantitative Proteomic Analysis—For the identification of the phosphorylation- and isoform-specific HNF4α peptide, MS/MS data were processed with Mascot® software (version 2.1.04, Matrix Science) against the NCBInr data base (AddGene Nr_Human 189494 sequences; Maze) at a peptide mass tolerance of 3 ppm and fragment mass tolerance of 0.8 Da, taking into account fixed peptide modification by carbamidomethyl (C), variable peptide modifications by methionine oxidation, as well as phosphorylation, including phosphoserine, phosphothreonine, and phosphotyrosine. The analysis of the data was carried out with Scaffold software (Proteome Software). For the label-free semiquantitative proteomic analysis, the SwissProt 57.3 *Homo sapiens* database (20,405 sequences) was used. The cut-off score was 35. The label-free semiquantitative values were determined using the Expressionist Refiner MS software (GeneData). After pre-processing (noise subtraction, RT alignment, and peak detection) and importing the identification results from the Mascot software, the relative ion intensities were calculated and normalized by the Lowess normalization method. The intensities of ions having the same calculated mass ±0.01 Da with different charges were summed.

Statistical Analyses—*p* values were calculated using two-way factorial analysis of variance.

Complex Analysis—First, the 302 complex lists containing the protein(s) with analysis of variance p values ≤ 0.000001, the assigned picomole in terms of both of the anti-HNF4α antibodies ≥0.05, and the assigned picomole in terms of control IgG ≤0.05, were extracted from the Human Protein Reference Database (HPRD) (37). Then, the complex lists in which the number of proteins in supplemental Data S1*C* was less than one-third and the assigned total picomole of both of the anti-HNF4α antibodies was less than 1 pmol, were excluded from the first 302 complex lists. Finally, the chosen complex lists were grouped by repeating the following procedure: the complex list that had the highest total assigned picomole of both the anti-HNF4α antibodies was picked; and the complex lists in which over one-half of the proteins were included in the picked complex were extracted and grouped.

Transient Transfection and Preparation of Whole Cell Lysate—The expression plasmid of human HNF4α isoform 2 was previously described (38). The human HNF4γ cDNA was cloned from HepG2 cell RNA and inserted into the pcDNA3 vector (Invitrogen). All of mutant HNF4α isoform 2 and HNF4γ plasmids were created with the QuikChange site-directed mutagenesis kit (Stratagene). CHO cells were grown as previously described (35). CHO cells were plated in 100-mm plates at 8×10^5 cells for 18 h prior to co-transfection. Co-transfection procedures were performed with the TransIT LT-1 transfection reagent (Mirus Bio LLC) using 4 μg each of the expression vector pairs per plate. After 48 h of co-transfection, cells were gently rinsed with ice-cold PBS, 0.2 mM PMSF and harvested by scraping into fresh ice-cold PBS, 0.2 mM PMSF. Harvested cells were collected by centrifugation for 10 min at 2,000 × *g* and lysed with lysis buffer (20 mM Tris-HCl, pH 7.5, 2 mM $MgCl_2$, 150 mM NaCl, 2 mM EGTA, 10% glycerol, 1% Nonidet P-40, 25 mM β-glycerophosphate,

10 mM NaF, 0.2 mM PMSF, 0.5 mM DTT, 1 protease inhibitor mixture tablet (Roche Applied Science) per 10 ml). Benzonase nuclease (Novagen) was added to the lysed cells at a final concentration of 25 units/ml and they were incubated on ice for 30 min. The lysate was centrifuged 15 min at 20,000 × *g* and the pellet was discarded and used for the subsequent IP.

Immunofluorescence—Immunofluorescence was performed as previously described (39). HepG2 cells plated on chamber slides were fixed with 4% (w/v) paraformaldehyde in PBS for 5 min, permeabilized with 0.5% (v/v) Triton X-100 in PBS for 5 min on ice, and blocked with PBS containing 10% normal goat serum. They were stained with antibodies anti-HNF4γ B6502A and anti-HNF4α F domain H1415 labeled with a Zenon Alexa Fluor 488 labeling kit (Invitrogen) in dilutions of 1:100 and 1:50, respectively. For the detection of B6502A, the Alexa Fluor 594 anti-mouse IgG Fab′ fragment (1:1000 dilution; Invitrogen) was used as a secondary antibody. Immunofluorescence was captured with a confocal laser scanning microscope (LSM510META; Carl Zeiss).

ChIP-qPCR, ChIP-reChIP-qPCR, ChIP Sequencing, and Data Analysis—For the ChIP analysis using antibodies anti-HNF4α F domain H1415, anti-HNF4α A/B domain K9218, and anti-HNF4γ B6502A, HepG2 cells were cross-linked with 1% formaldehyde for 10 min at room temperature and prepared for ChIP as described previously (40). For ChIP-reChIP, the elution step was carried out by adding the elution buffer with 10 mM DTT for 30 min at 37 °C after the 1st ChIP. The eluted samples were diluted 40 times with ChIP dilution buffer, and the reChIP was then performed by adding the 2nd antibody. ChIP and ChIP-reChIP samples were also analyzed by gene-specific quantitative real time PCR (qPCR) analyses. The primer sequences used for ChIP-qPCR are shown under supplemental Table S1. ChIP-seq sample preparation for sequencing was performed according to the manufacturer's instructions (Ilumina). Sequences were mapped to the Build #37 reference human genome. As a result, 6,928,104, 6,980,254, and 6,631,466 sequences were uniquely mapped for antibodies anti-HNF4α F domain H1415, anti-HNF4α A/B domain K9218, and anti-HNF4γ B6502A, respectively. A Genomatix bioinformatics software package was used to search for the sequence motifs enriched among the sequences having HNF4 binding. The 1000 bp sequences around the position with the highest binding *p* value in each gene group were used. We applied the CoreSearch tool (41) to the top 50 sequences from the highest signal rates in the ChIP-seq data for the determination of the preliminarily motifs. Using these generated preliminarily motifs, similar sequences were extracted from the top 1000 sequences with the highest signal rates in the ChIP-seq data using the MatInspector search tool (42). The final motifs were generated with the MatDefine tool (42) using the frequency of the extracted sequences from MatInspector.

RNA Interference—The duplex constructs for each small interfering RNA (siRNA) targeting HNF4α mRNA, *i.e.* 4α-(i) and 4α-(ii), along with the negative control, 4α-control (negative control siRNA), were purchased from Qiagen. The duplexes for each siRNA targeting HNF4γ mRNA, *i.e.* 4 γ-(i), and 4 γ-(ii), along with the negative control, 4γ-control (Stealth RNAi Negative Control Kit with Midium GC), were purchased from Invitrogen. These target sequences are shown under supplemental Table S1. For transfection, 2.5×10^5 HepG2 cells in a 6-well plate were transfected with 10 nM of each siRNA along with Lipofectamine RNAi MAX reagent (Invitrogen) according to the manufacturer's instructions. After a 48-h transfection, HNF4α and HNF4γ expression activities were confirmed by immunoblotting and quantitative real time PCR.

Quantitative Real Time PCR—RNA was reverse-transcribed using a first-strand cDNA synthesis kit (Invitrogen) and subsequently assayed by quantitative real time PCR with an ABI PRISM 7900HT sequence detection system (Applied Biosystems). All of the primer sequences are shown in supplemental Table S1. Cyclophilin mRNA was used as an internal control in all studies.

Microarray Analysis—Microarray expression analysis was performed using the Affymetrix GeneChip system according to the manufacturer's instructions. Labeled cRNA probes were hybridized to Affymetrix U133plus 2.0 arrays (Affymetrix). The microarray imaging data were scanned and analyzed with GeneChip Operating Software (Affymetrix).

Accession Numbers—We have deposited the microarray datasets and ChIP-seq datasets in the GEO data base (accession number GSE18990).

Luciferase Reporter Assay—The luciferase reporter assay was carried out as previously described (35). The positions −1 to −204 relative to the translation start site of the cell death-inducing DFFA-like effector b (*CIDEB*) and the 5′ UTR of the *HGD* gene were amplified by PCR, using human genomic DNA from HepG2 cells as a template, and cloned into the luciferase reporter vector, pGL3 basic (Promega). The resulting constructs were designated CIDEB-(1–204) and HGD 5′ UTR. Mutations were introduced by PCR-based site-directed mutagenesis, using a QuikChange site-directed mutagenesis kit (Stratagene) according to the manufacturer's protocol. The mutation sequences were as follows: for the CIDEB-(1–204) of the distal DR1 motif (bp −174 to −162), from AGGGCAAAGTCCA to AGGGGATCCTCCA; for the CIDEB-(1–204) of the proximal DR1 motif (bp −142 to −130), from GGGCCAGAGTCCA to GGGCGGATCCCCA; for the HGD 5′ UTR of DR1 motif (bp −191 to −179), from GGGAGAAAGTCCA to GGGGGATCCTCCA. HEK293 cells were grown as previously described (35). For transfection, HEK293 cells were plated at a density of 0.5×10^5/24-well plate on the day before transfection. On day 1, cells were transfected with a luciferase reporter plasmid (50 ng), the expression plasmids (75 ng), and pRL-TK (5 ng) using the Lipofectamine 2000 reagent (Invitrogen) according to the manufacturer's instructions. The total amount of DNA per well was kept constant by adding the corresponding amount of the expression vector without a cDNA insert. On day 2, the preparation of cell lysates and measurements of the luciferase activity were performed using the Dual Luciferase Reporter assay system (Promega) according to the manufacturer's instructions. All assays were performed twice in triplicate.

Electrophoresis Gel Mobility Shift Assay (EMSA)—EMSAs were carried out as described previously (43). Double-stranded oligonucleotides were labeled with [α-^{32}P]dCTP and

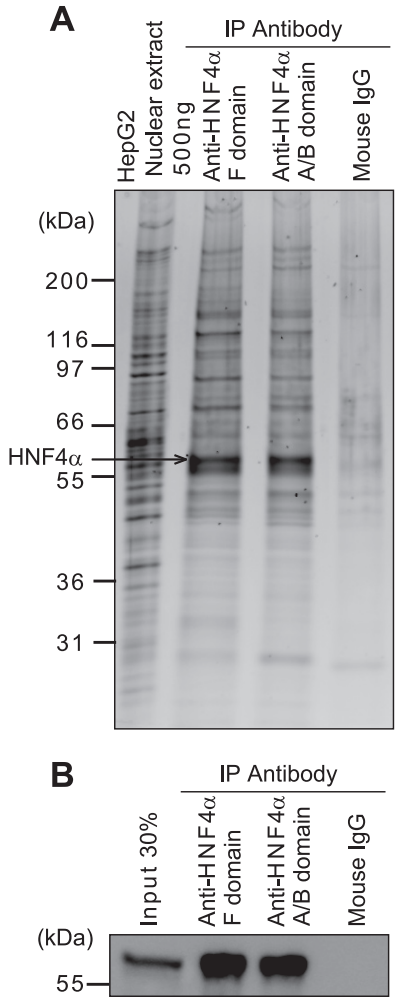

FIGURE 1. **Immunoprecipitation of native HNF4α and its interactive proteins.** The immunoprecipitated native HNF4α and its complexes from HepG2 nuclear extract were (*A*) stained with SYPRO Ruby protein staining and (*B*) immunoblotted with the H1415 horseradish peroxidase (HRP)-conjugated anti-HNF4α F domain antibody. From a single gel band, pointed out by the *arrow* in *A*, HNF4α was identified by database search and inspection of individual MS/MS spectra in the raw files.

a Klenow fragment, and purified using a G-50 microspin column (GE Healthcare). The oligonucleotide sequences used for the probes and competitors are shown in supplemental Table S1. For supershift experiments, nuclear extracts were preincubated with each of the anti-HNF4 antibodies and mouse IgG for 20 min at room temperature.

RESULTS

Strategy for the Proteomic Analysis of the Native HNF4α Status—To clarify the transcriptional control of HNF4α and its cofactor complex in the steady-state native condition, HNF4α was immunopurified from HepG2 nuclear extract (Fig. 1) and analyzed using highly sensitive shotgun proteomics. Two domain-specific monoclonal antibodies (mAbs) were chosen for IP, one that recognizes the F domain (Clone number H1415) and one that recognizes the A/B domain (Clone number K9218). Each of these mAbs was cross-linked to Protein G-conjugated magnetic beads developed by JSR Corporation for IP. The protein staining and immunoblotting indicated that the IP quality was of low noise and high yield (Fig. 1). Using in-gel digestion following liquid chromatography coupled tandem mass spectrometry (LC/MS/MS), the most intense band was identified as HNF4α isoform 2 (indicated by the *arrow* in Fig. 1*A*). One milligram of HepG2 nuclear extract was calculated to contain 11.3 pmol of HNF4α from the immunoblot intensity, using the GST fusion HNF4α E-F domain protein as the calibrator. For more detailed analysis, three independent HepG2 nuclear extracts were immunoprecipitated with two mAbs in triplicate, and all samples were subjected to gel-free LC/MS/MS. The HNF4α phosphorylation and isoforms were identified using an MS/MS database search, and the amount of various HNF4α associating cofactors was evaluated with label-free semiquantitative proteomic analysis (44), using a reported method in which the average of the three highest peptide intensities in each protein was regarded as the relative abundance of the protein (45).

Proteomic Identification of the Native HNF4α Isoform and Phosphorylation Status—Utilizing a MASCOT database search, three phosphorylated peptides were found in HNF4α (Fig. 2*A*). Upon inspection of each of the MS/MS spectra in the raw files, either of the reported phosphorylation sites of Ser^{133} and Ser^{134} (17), together with Ser^{158} (15), were confirmed. Additionally, the phosphorylation of Ser^{427}, and the double phosphorylation of Thr^{420} + Ser^{427}, were newly identified from the MS/MS neutral loss ion spectra (Fig. 2*B* and supplemental Fig. S1). In terms of other HNF4α modifications, ubiquitination of Lys^{224} was observed. Certain isoform-specific peptides, *i.e.* the P2 promoter driven A/B domain (*green box*), 10 amino acid inserted F domain (*blue box*), and F domain variant produced by extension of the last exon encoding the E domain (*yellow box*), were identified (Fig. 2*C*). It is therefore suggested that the native HNF4α isoform engages in heterodimer formation, because H1415 lacks reactivity against isoforms 3 and 9, and K9218 lacks reactivity against isoforms 7, 8, and 9, respectively (38). The results of immunoblotting with HNF4α-isoform-specific mAbs demonstrated the existence of all of the isoforms except 9, and the co-IP of heterogeneous isoforms in HepG2 cells (Fig. 2*D*).

Proteomic Landscape of Functional HNF4α Associating Cofactors—The relative abundance of the identified proteins was calculated from the average peak intensities of the peptides identified in each IP to obtain a comprehensive analysis of the HNF4α cofactors (supplemental Data S1, *A* and *B*). Using these relative abundances, the statistical significance (analysis of variance *p* value) between the anti-HNF4α and control IP was assessed, and each relative amount was normalized, with the average amount of HNF4α being 11.3 pmol (supplemental Data S1, *B* and *C*). Among these, several of the HNF4α interacting factors listed in the PubMed Gene database were observed (Table 1). From the newly identified proteins, we extracted HNF4α associating cofactor candidate complexes from the HPRD, and grouped the overlapping complexes (see "Experimental Procedures"). Among the categorized complexes, we identified the DNA-dependent protein kinase catalytic subunit (DNA-PKcs), HAT complex SPT3-TAF_{II}31-GCN5L acetylase (STAGA) and Tip60 HAT com-

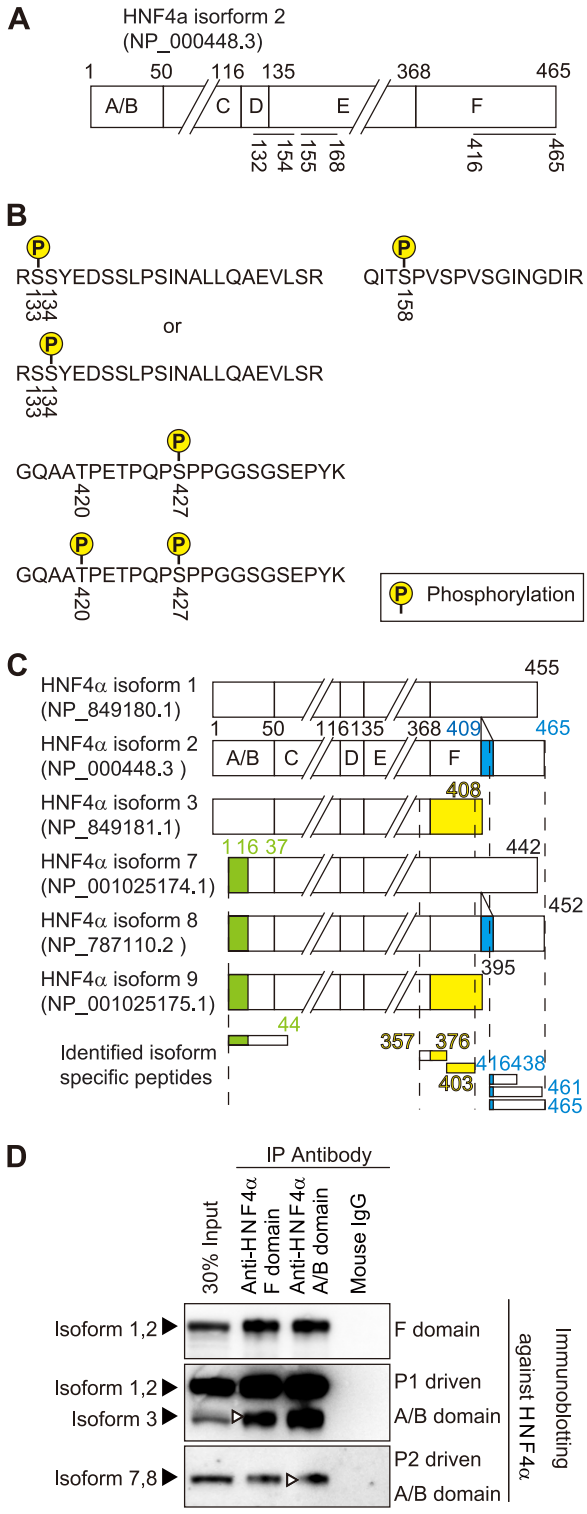

FIGURE 2. **Identification of steady-state native HNF4α phosphorylation and isoforms.** *A*, schematic illustration of the identified regions of HNF4α phosphorylation. The *box* represents the domain structure of human HNF4α isoform 2. The *numbers above* the box represent the amino acid number in each domain. The regions and amino acid number corresponding to phosphorylation are represented by *lines* and the *numbers under* the *box*, respectively. *B*, the identified sites of native HNF4α phosphorylation. The identified phosphorylated peptides in human HNF4α isoform 2 are represented by *single letter* notation of the amino acid, and phosphorylated residues are represented by *yellow circles*. *C*, schematic illustration of the identified peptides that correspond to the HNF4α isoforms. The *upper six boxes* represent the domain structure of the human HNF4α isoforms. The *lower bars* represent the identified isoform-specific peptides. Each *colored region* indicates the isoform-specific amino acid residues that were identified by proteomic analysis. *D*, physical conformation of the native HNF4α isoform heterodimer. HepG2 nuclear extract was used for immunoprecipitation. Immunoblotting was carried out using the horseradish peroxidase (HRP)-conjugated anti-HNF4α F domain antibody H1415, anti-HNF4α P1 driven A/B domain antibody K9218, and anti-HNF4α P2 driven A/B-domain antibody H6939. The bands indicated by the *open arrowheads* are the HNF4α isoforms that did not react with the monoclonal antibodies used for immunoprecipitation.

plex (46, 47), U2 snRNP splicing complex (48), NR coactivator NCoA62/SKIP (49), vitamin D receptor-coupled chromatin remodeling complex WINAC (50), and nucleosome remodeling and histone deacetylation complex Mi-2/nucleosome remodeling and deacetylase (51) (Table 1). Various other novel associating proteins were also observed (Table 1). We confirmed the specificity and appearance of some of the noteworthy proteins listed in Table 1 by IP-immunoblotting with the available antibodies (supplemental Fig. S2).

Investigation of Functional HNF4α and HNF4γ Heterodimerization, and Transcriptional Activation in HepG2 cells—The HNF4 orphan superfamily member HNF4γ (HNF4G) was unexpectedly found to be one of the most evident of the associating proteins (Table 1). We confirmed that there were HNF4γ-specific peptides (supplemental Fig. S3*A*), and the possibility of a cross-reaction between anti-HNF4α and -γ mAbs was excluded (supplemental Fig. S3*B*). Thus, we focused on the possibility of transcriptional regulation by the HNF4α-HNF4γ heterodimer. The co-IP analysis of native HNF4α and HNF4γ confirmed the interaction (Fig. 3*A*). The pull-down analysis of the mutated $K(X)_{26}E$ motif for HNF4α and HNF4γ revealed the importance of the heterodimerization through the $K(X)_{26}E$ motif for each of them (Fig. 3, *B* and *C*). Immunofluorescence analysis indicated partial co-localization in the nucleus (Fig. 3*D*). These biochemical analyses reveal native HNF4α-HNF4γ to be a heterodimer.

To elucidate the gene regulatory mechanism of the HNF4α-HNF4γ heterodimer, chromatin immunoprecipitation sequencing (ChIP-seq) analysis with anti-HNF4α and HNF4γ mAbs (Fig. 4*A*) as well as microarray analysis of the siRNA-mediated HNF4α and HNF4γ double knockdown (Fig. 4*B* and supplemental Data S2) were performed using HepG2 cells. An analysis of the HNF4α and/or HNF4γ binding DR1 sequence frequencies did not reveal any definitive differences, but did indicate a few variations in the consensus DR1 sequence (Fig. 4*C*). Next, we analyzed the correlation between the ChIP-seq binding genes and microarray expression profiles based on the reported method by Wang *et al.* (52). Although the gene groups of HNF4α-HNF4γ overlap and HNF4α did exhibit a correlation between the ChIP-seq binding intensity and the activation of certain genes, the correlation was less conspicuous in the HNF4γ gene groups (Fig. 4*D*). To determine whether the HNF4α-HNF4γ heterodimer activates transcription, we selected two candidate genes from the HNF4α-HNF4γ overlapping group, the *CIDEB* short transcript (53, 54) and the homogentisate 1,2-dioxygenase (*HGD*) gene (55).

TABLE 1

Proteomic identification of HNF4α associating complexes and cofactors

The category grouping of HNF4α association cofactors is performed as described under "Experimental Procedures." "Both" means extracted from both of the HNF4α antibody-specific proteins, the "F domain" is extracted from the HNF4α F domain antibody H1415 only proteins, and the "A/B domain" is extracted from HNF4α A/B domain antibody K9218 only proteins, respectively. The quantitative and motif data sets were assigned from supplemental Data S1C.

	Protein name		Average amount (pmol)					
Category	UniProt Entry Name	Gene symbol	Immuno-precpitation with anti- F domain of HNF4α antibody	Immuno-precpitation with anti- A/B domain of HNF4α antibody	Immuno-precpitation with control IgG	Number of LXXLL motif	Number of LXX I/H IXXX I/L motif	Reference
HNF4α	HNF4A_HUMAN	HNF4A	7.518	11.300	0.005	-	-	
Reported HNF4α interactans	CBP_HUMAN	CREBBP	0.021	0.061	0.033	3	0	Pubmed Gene
	MED1_HUMAN	MED1	0.002	0.006	0.000	2	0	
	MED14_HUMAN	MED14	0.007	0.013	0.000	2	0	
	TCP4_HUMAN	SUB1	0.006	0.006	0.000	0	0	
	CTNB1_HUMAN	CTNNB1	0.014	0.017	0.004	5	0	
	MED16_HUMAN	MED16	0.015	0.019	0.000	5	0	
	MED24_HUMAN	MED24	0.004	0.005	0.000	6	1	
	PABP4_HUMAN	PABPC4	0.028	0.030	0.001	0	0	
	RAD50_HUMAN	RAD50	0.007	0.009	0.000	1	0	
DNA-PKcs complex	ANDR_HUMAN	AR	-	-	-	-	-	(58)
	PRKDC_HUMAN	PRKDC	0.090	0.085	0.009	16	0	
	RPB1_HUMAN	POLR2A	-	-	-	-	-	
	PARP1_HUMAN	PARP1	0.263	0.319	0.049	3	0	
	TOP1_HUMAN	TOP1	0.037	0.057	0.004	0	0	
	KU86_HUMAN	XRCC5	0.068	0.065	0.005	0	1	
	KU70_HUMAN	XRCC6	0.089	0.093	0.008	1	0	
STAGA complex	GCNL2_HUMAN	KAT2A	0.039	0.050	0.033	2	0	STAGA complex ; GO:0030914
	SF3B3_HUMAN	SF3B3	0.201	0.202	0.071	0	0	
	SUPT3_HUMAN	SUPT3H	0.017	0.023	0.004	2	0	
	ST65G_HUMAN	SUPT7L	0.048	0.061	0.005	0	0	
	TAD1L_HUMAN	TADA1L	0.048	0.071	0.010	0	0	
	TAD3L_HUMAN	TADA3L	0.039	0.063	0.012	2	0	
	TAF10_HUMAN	TAF10	0.030	0.032	0.002	0	0	
	TAF12_HUMAN	TAF12	-	-	-	-	-	
	TAF5L_HUMAN	TAF5L	0.020	0.031	0.005	0	0	
	TAF6L_HUMAN	TAF6L	0.027	0.038	0.007	1	1	
	TAF9_HUMAN	TAF9	0.013	0.019	0.002	0	0	
	TRRAP_HUMAN	TRRAP	0.111	0.115	0.018	9	1	
Tip60 complex	ACTB_HUMAN	ACTB	0.299	0.437	0.075	0	0	NuA4 histone acetyltransferase complex ; GO:0035267
	ACL6A_HUMAN	ACTL6A	0.043	0.065	0.003	0	0	
	BRD8_HUMAN	BRD8	0.021	0.018	0.000	1	0	
	DMAP1_HUMAN	DMAP1	0.019	0.019	0.001	0	0	
	EP400_HUMAN	EP400	0.022	0.015	0.001	1	0	
	E41L2_HUMAN	EPB41L2	0.038	0.081	0.024	0	0	
	ING3_HUMAN	ING3	0.021	0.018	0.000	0	0	
	TIP60_HUMAN	KAT5	0.004	0.003	0.000	1	0	
	CA149_HUMAN	MEAF6	0.013	0.013	0.000	0	0	
	MO4L1_HUMAN	MORF4L1	0.013	0.013	0.004	1	0	
	RUVB1_HUMAN	RUVBL1	0.306	0.852	0.126	0	0	
	RUVB2_HUMAN	RUVBL2	0.169	0.249	0.036	1	0	
	TRRAP_HUMAN	TRRAP	0.111	0.115	0.018	9	1	
	YETS4_HUMAN	YEATS4	0.007	0.005	0.000	1	0	
U2 snRNP complex	SF3B1_HUMAN	SF3B1	0.077	0.050	0.003	3	1	(48)
	SF3B2_HUMAN	SF3B2	0.035	0.022	0.002	0	0	
	SF3B3_HUMAN	SF3B3	0.201	0.202	0.071	0	0	
	SF3A1_HUMAN	SF3A1	0.075	0.047	0.012	0	0	
	SF3A3_HUMAN	SF3A3	0.030	0.021	0.003	1	0	
	SF3B4_HUMAN	SF3B4	0.006	0.007	0.000	0	0	
	SMN_HUMAN	SMN1	0.025	0.021	0.003	1	0	
	RU2A_HUMAN	SNRPA1	0.033	0.025	0.001	2	0	
	RU2B_HUMAN	SNRPB2	0.067	0.045	0.003	0	0	
	RSMB_HUMAN	SNRPB	0.031	0.023	0.002	0	0	
	SMD3_HUMAN	SNRPD3	0.210	0.207	0.053	0	0	
	SMD2_HUMAN	SNRPD2	0.041	0.031	0.004	0	0	
	SMD1_HUMAN	SNRPD1	0.254	0.229	0.014	1	0	
	RUXF_HUMAN	SNRPF	0.012	0.008	0.001	0	0	
	DDX46_HUMAN	DDX46	0.001	0.001	0.000	1	0	
	SPT2_HUMAN	SPTY2D1	0.011	0.029	0.021	0	0	
	CHERP_HUMAN	CHERP	0.001	0.002	0.000	0	0	
	DHX15_HUMAN	DHX15	0.054	0.036	0.002	0	0	
	TRAP1_HUMAN	TRAP1	0.118	0.113	0.020	4	0	
	PUF60_HUMAN	PUF60	0.060	0.051	0.004	0	0	
	U2AF2_HUMAN	U2AF2	0.135	0.149	0.019	0	0	
	CH60_HUMAN	HSPD1	0.026	0.027	0.009	0	0	
	SPF45_HUMAN	RBM17	0.012	0.028	0.027	0	0	
	U2AF1_HUMAN	U2AF1	0.049	0.055	0.003	0	0	
	HM20A_HUMAN	HMG20A	0.008	0.004	0.000	0	0	
	DNJC8_HUMAN	DNAJC8	0.009	0.006	0.000	0	0	
	SFRS1_HUMAN	SFRS1	0.017	0.010	0.000	0	0	

TABLE 1—*continued*

Category	Protein name		Average amount (pmol)			Number of LXXLL motif	Number of LXX I/H IXXX I/L motif	Reference
	UniProt Entry Name	Gene symbol	Immuno-precpitation with anti- F domain of HNF4α antibody	Immuno-precpitation with anti- A/B domain of HNF4α antibody	Immuno-precpitation with control IgG			
NCoA62/SKIP complex	EF1A1_HUMAN	EEF1A1	0.120	0.150	0.043	0	0	(49)
	SNW1_HUMAN	SNW1	0.005	0.005	0.003	0	0	
	GRP78_HUMAN	HSPA5	0.711	1.020	0.227	0	0	
	K6PL_HUMAN	PFKL	0.002	0.002	0.000	0	0	
	TBB5_HUMAN	TUBB	0.547	0.651	0.124	0	0	
	TBB4_HUMAN	TUBB4	0.003	0.005	0.000	0	0	
	HNRPU_HUMAN	HNRNPU	0.887	2.009	0.406	1	0	
	MATR3_HUMAN	MATR3	0.733	1.140	0.248	0	0	
	UBR5_HUMAN	UBR5	0.000	0.000	0.000	5	0	
	SFPQ_HUMAN	SFPQ	0.848	1.479	0.132	0	0	
	DDB1_HUMAN	DDB1	0.005	0.008	0.000	1	0	
	EF1G_HUMAN	EEF1G	-	-	-	-	-	
WINAC complex	SMCA4_HUMAN	SMARCA4	-	-	-	-	-	(50)
	BAZ1B_HUMAN	BAZ1B	0.013	0.019	0.002	4	0	
	ARI1A_HUMAN	ARID1A	-	-	-	-	-	
	SNF5_HUMAN	SMARCB1	-	-	-	-	-	
	SMRC2_HUMAN	SMARCC2	0.023	0.030	0.001	1	0	
	SMRC1_HUMAN	SMARCC1	0.011	0.015	0.001	1	0	
	SP16H_HUMAN	SUPT16H	0.045	0.047	0.002	0	0	
	CAF1A_HUMAN	CHAF1A	-	-	-	-	-	
	VDR_HUMAN	VDR	-	-	-	-	-	
	SMCE1_HUMAN	SMARCE1	0.002	0.002	0.000	0	0	
	ACL6A_HUMAN	ACTL6A	0.043	0.065	0.003	0	0	
	SMRD1_HUMAN	SMARCE1	-	-	-	-	-	
	TOP2B_HUMAN	TOP2B	0.435	0.577	0.015	1	0	
	SMCA2_HUMAN	SMARCA2	-	-	-	-	-	
NuRD complex	CHD3_HUMAN	CHD3	0.036	0.063	0.012	4	0	NuRD complex ; GO:0016581
	CHD4_HUMAN	CHD4	0.154	0.272	0.100	3	0	
	CSK21_HUMAN	CSNK2A1	0.006	0.010	0.001	1	0	
	P66A_HUMAN	GATAD2A	0.191	0.328	0.176	0	0	
	HDAC1_HUMAN	HDAC1	0.042	0.111	0.023	0	0	
	HDAC2_HUMAN	HDAC2	0.003	0.013	0.001	0	0	
	MBD3_HUMAN	MBD3	0.002	0.005	0.000	0	0	
	MTA1_HUMAN	MTA1	0.019	0.037	0.001	0	0	
	MTA2_HUMAN	MTA2	0.027	0.039	0.026	0	0	
	RBBP4_HUMAN	RBBP4	0.384	0.646	0.199	0	0	
	RBBP7_HUMAN	RBBP7	0.011	0.027	0.004	0	0	
Both	HNF4G_HUMAN	HNF4G	0.279	0.288	0.001	1	0	
	PELP1_HUMAN	PELP1	0.144	0.278	0.026	13	0	
	LAP2A_HUMAN	TMPO	0.065	0.067	0.006	0	0	
	LMNA_HUMAN	LMNA	0.013	0.014	0.003	1	0	
	BAF_HUMAN	BANF1	0.010	0.009	0.000	0	0	
F_domain	PERQ2_HUMAN	GIGYF2	0.756	0.033	0.005	1	0	
	JAD1A_HUMAN	KDM5A	0.231	0.294	0.033	2	0	
AB_domain	LSD1_HUMAN	KDM1	0.067	0.168	0.035	1	0	
	JHD2C_HUMAN	JMJD1C	0.065	0.129	0.045	2	0	
other	EP300_HUMAN	EP300	0.032	0.060	0.011	3	0	(71)
	EWS_HUMAN	EWSR1	0.826	0.770	0.091	0	0	(73)

These genes were down-regulated by HNF4α and HNF4γ double knockdown, and ChIP-seq and ChIP-reChIP binding was observed (Fig. 5, *A–C*). Additionally, the candidate DR1 sites, which were the same as the identified motifs of the HNF4α-HNF4γ heterodimer, were found in each ChIP-seq binding region (Fig. 5*D*). We checked the promoter activity of each region by reporter assay. In CIDEB-(1–204), a slight luciferase activity in the distal region of DR1 was observed, whereas the proximal region of DR1-dependent luciferase activity was the most pronounced with both HNF4α and HNF4γ synergistically (Fig. 5*E*). The DR1-dependent luciferase activity induced by HNF4α and HNF4γ was also observed in the HGD 5′ UTR (Fig. 5*E*). Finally, the *in vitro* DR1 site binding of the HNF4α-HNF4γ heterodimer was confirmed by EMSAs (Fig. 5*F*). These results suggest a synergistic activation of HNF4α and HNF4γ at the same DR1 site in both the CIDEB-(1–204) and HGD 5′ UTR regions.

DISCUSSION

One of the main functions of HNF4α is the constitutive regulation of genes in critical metabolic pathways of the liver (14, 56), thus we performed a proteomic analysis of steady-state native HNF4α to elucidate the mechanisms of fine tuning of multiple transcriptional activities. The use of domain-specific mAbs allowed incremental improvement of proteomic analysis reliability and covered all of the HNF4α isoforms except isoform 9. The results of IP using these mAbs showed a high signal-to-noise ratio (Fig. 1). The major expression of HNF4α isoform 2 is consistent with the expression in the human liver (57). High sensitivity shotgun proteomics identified the isoforms and phosphorylation status of native HNF4α (Fig. 2). Among the major identified phosphorylation sites, a novel site, which corresponds to a 10-amino acid insert F domain, is expected to be able to modulate transcriptional activity by a

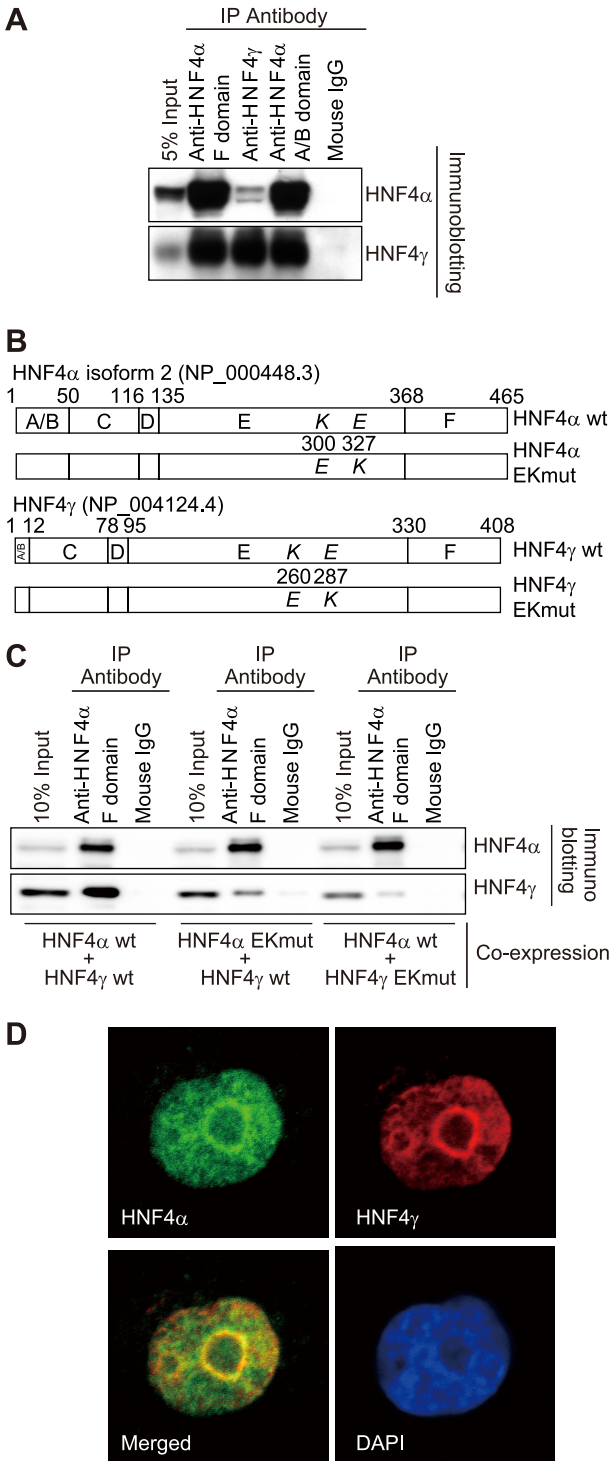

FIGURE 3. **Physical conformation of the native HNF4α and HNF4γ heterodimerization.** *A*, physical interaction of native HNF4α and HNF4γ. HepG2 nuclear extract was used for immunoprecipitation. *B*, schematic diagrams of the HNF4α and HNF4γ mutation constructs. The *box* represents the domain structure of human HNF4α isoform 2 and HNF4γ. The *numbers above the box* represent the amino acid number in each domain. *C*, the pull-down assays of the co-expressed HNF4α and HNF4γ in combination with the heterodimerizing mutation. *D*, localization of the native HNF4α and HNF4γ in HepG2 cells by immunofluorescence staining. HepG2 cells were visualized with the anti-HNF4α F domain monoclonal antibody H1415 (*green*) and the anti-HNF4γ monoclonal antibody B6502A (*red*). The *left bottom panel* shows the merged image of HNF4α and HNF4γ. HepG2 cells were also visualized by 4,6-diamidino-2-phenylindole (*DAPI*) staining (*blue*). All immunoprecipitation results were subjected to immunoblotting using HRP-conjugated antibodies H1415 and B6502A.

conformational change and/or recruiting specific cofactors (Fig. 2*B*) (25). The identification of multiple phosphorylation sites suggests a contribution to the multiple functional roles of HNF4α through changes in phosphorylation. The identified inter-isoforms suggested isoform heterodimerization (Fig. 2*C*), which was confirmed by immunoblotting (Fig. 2*D*). These results imply the possibility that all of the isoforms form heterodimers, and also that there is a fine tuning of transcriptional regulation by an HNF4α isoform homodimer or heterodimer.

In an effort to determine the proteomic landscape of the HNF4α interacting factors and complexes using the identified proteins and protein complex database in HPRD, we categorized the cofactor complexes by function and stoichiometry (Table 1). Among the outstanding complexes, the DNA-PKcs has already been reported as an NR cofactor (58). In relation to HNF4α, DNA-PK acts as the cofactor of FoxA2, which activates apolipoprotein AI in synergy with HNF4α (59). Because FOXA2 was found in our proteomic analysis as well, DNA-PKcs can be considered to be an HNF4α cofactor complex. We also found the HAT complexes. Because two HAT catalytic proteins, Gcn5-related HAT Gcn5L (KAT2A) and MYST-related HAT TIP60 (KAT5) were identified, the STAGA and Tip60 HAT complexes (46, 47) might function as an HNF4α interacting complex. In a previous report of STAGA complex identification, SF3B3 was found to be a STAGA subunit (47). In addition to SF3B3, we identified SF3B3 containing the U2 snRNP splicing complex, supporting the concept of a coupling of transcriptional activation and mRNA splicing. Recent investigation revealed that STAGA subunits of ATXN7L3, USP22, and ENY2 act as both histone H2A/B-deubiquitination modules and NR cofactors (60). Although these reported subunits were not found in our results, H2A/B and ubiquitin-specific protease USP10 (UBP10) were identified (supplemental Data S1*C*), so it may indeed be a candidate partner of the HNF4α characteristic STAGA subunit of the H2A/B-deubiquitination modules. As already reported for other NR cofactor complexes, NCoA62/SKIP (49), WINAC (50), and nucleosome remodeling and deacetylase (51) were identified here. These complexes can also be regarded as HNF4α cofactors in HepG2 cells. Among the proteins that were not assigned to the HPRD complex, we observed steroid receptor cofactor proline-, glutamic acid- and leucine-rich protein 1 (PELP1), a typical NR cofactor with an L*XX*LL coactivator motif (61), and Lamina-associated polypeptide 2 isoform α (TMPO), with Lamin A (LMNA) and BAF (BANF1), which are related to the nuclear matrix association and chromosome structure (62). We also observed lysine-specific histone demethylase 1 (KDM1) and lysine-specific demethylase 5A (KDM5A), which are the demethylases of the 4th lysine residue of histone H3 (63, 64), and probable jmjC domain-containing histone demethylyation protein 2C (JMJD1C), which is the demethylase of the 9th lysine residue of histone H3 (65). Because these proteins have been reported as NR binding partners (65, 66), they might function as an HNF4α-mediating epigenetic control. Recently, KDM1 was

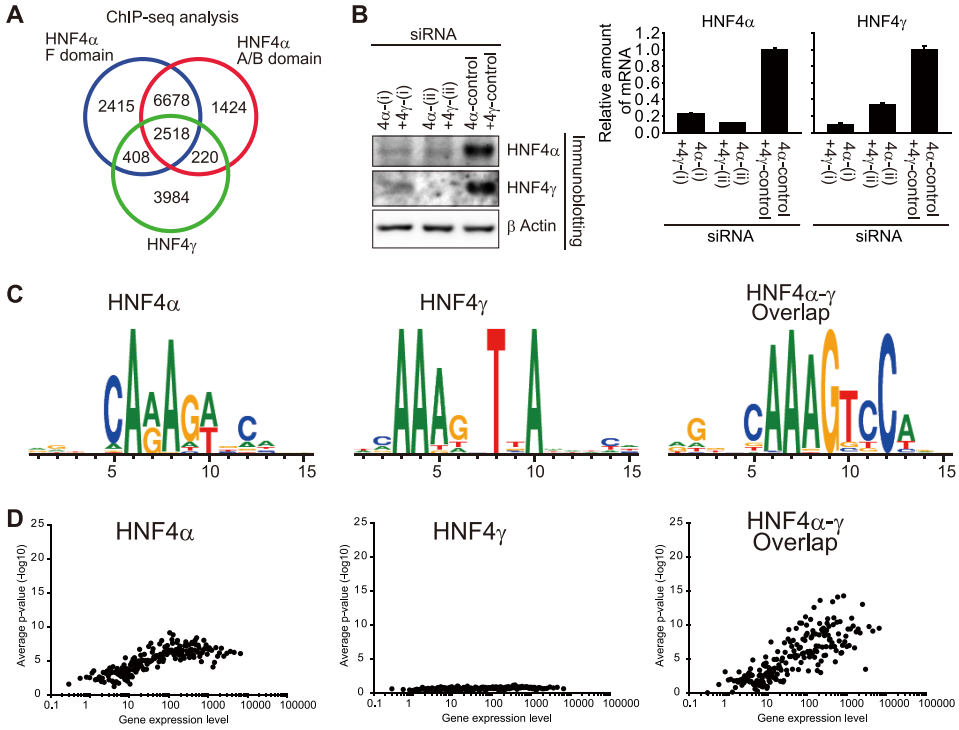

FIGURE 4. **Genome-wide analysis of HNF4α and HNF4γ binding genes and the regulation of their expression in the steady-state.** *A*, venn diagrams of HNF4α and HNF4γ co-localization (gene body and −/+ 20,000 base pairs surrounding the gene body) by ChIP-seq analyses. The *circles* designate the genes for which the signal is observed with each antibody. The *numbers* in each set denote the number of genes. The *overlapping region* indicates that signal overlap is observable. *HNF4α F-domain* (*blue*), anti-HNF4α F domain antibody H1415; *HNF4α A/B-domain* (*red*), anti-HNF4α A/B domain antibody K9218; *HNF4γ* (*green*), anti-HNF4γ antibody B6502A. *B,* siRNA-mediated HNF4α and HNF4γ double knockdown. HepG2 cells were transfected with either HNF4α and -γ-specific siRNAs (4α+4γ) or control siRNA (control). After transfection, the cells were harvested for the isolation of total RNA and whole cell lysate. *C,* identification of enriched motifs in the HNF4 binding sequence. The *height of each letter* represents the relative frequency of nucleotides at different positions in the consensus region. *D,* the correlations between each of the HNF4 binding levels and gene expression. Averages of the microarray expression dataset of the control siRNA-transfected HepG2 cells were used for the steady-state HepG2 expression level. Genes were grouped as 100 gene sets (*one dot* in the figure) according to the steady-state expression level. Each HNF4 binding level was calculated for the same 100 gene sets. The *y* axis indicates the HNF4 binding level, and the *x* axis indicates the steady-state expression level.

reported as a newly identified nucleosome remodeling and deacetylase subunit (67), but it is still not in the HPRD. In terms of the most conspicuous difference between the domain-specific mAbs, the PERQ amino acid-rich with GYF domain-containing protein 2 (GIGYF2) should be noted as a new candidate for A/B domain binding (supplemental Fig. S2). GIGYF2 has been reported to be a transiently binding protein to the insulin-like growth factor 1 receptor and a modulator of insulin-like growth factor-1 signaling, with two nuclear localization signals and one L*XX*LL motif (68). Considering the HNF4α mutation in MODY1 lacking the NH_2-terminal transactivation domain (9) and the postulated linkage between HNF4α and the insulin/insulin-like growth factor-1 signaling pathway in diabetes (69), GIGYF2 is an important candidate for regulation of glucose metabolism in the liver. The reported HNF4α cofactors EWS (70) and p300 (71) were also observed, although with a low level of reliability. Together, the results suggest the importance of the HNF4α mediating functional complexes and help bring into focus the dynamic proteomic landscape, especially in terms of extracellular/intracellular signaling and/or the developmental cascade. They do not, however, answer the question of whether any of the identified proteins intrinsically formed the complex with HNF4α, because some of the proteins may have formed interactive complexes after dialysis with the high to low salt condition in the course of nuclear extract preparation. However, we observed that HNF4γ, part of the Tip60 complex, PELP1, Lamina-associated polypeptide 2 isoform α, and GIGYF2 were also identified by proteomic analysis under a high salt wash condition. These proteins thus seem to be natural and high affinity HNF4α interacting factors.

HNF4α has been considered to act almost exclusively as a homodimer (34). In this study, however, the analysis of the native HNF4α complex revealed much greater complexity, including heterodimerization with HNF4γ (Fig. 3), which suggests multiple stages of fine regulation of transcription. Two candidate genes for HNF4α-HNF4γ heterodimer regulation, the lipogenesis- and fatty acid oxidation-controlling factor *CIDEB* (54) and the key enzyme in the tyrosine and phenylalanine metabolic pathways, *HGD* (55), were selected from the ChIP-seq and microarray analyses. These analyses proved to be highly useful for predicting the active binding sites and revealing transcriptional activation by the heterodimer (Figs. 4 and 5). Our finding shows that the HNF4α-γ heterodimer activates certain genes involved in the control of metabolism (Fig. 5).

The proteomic analysis described here was performed using the nuclear extract of single dish-cultured cells. Applying this highly sensitive proteomic method, together with a semi-quantitative strategy for identifying the dynamic changes of

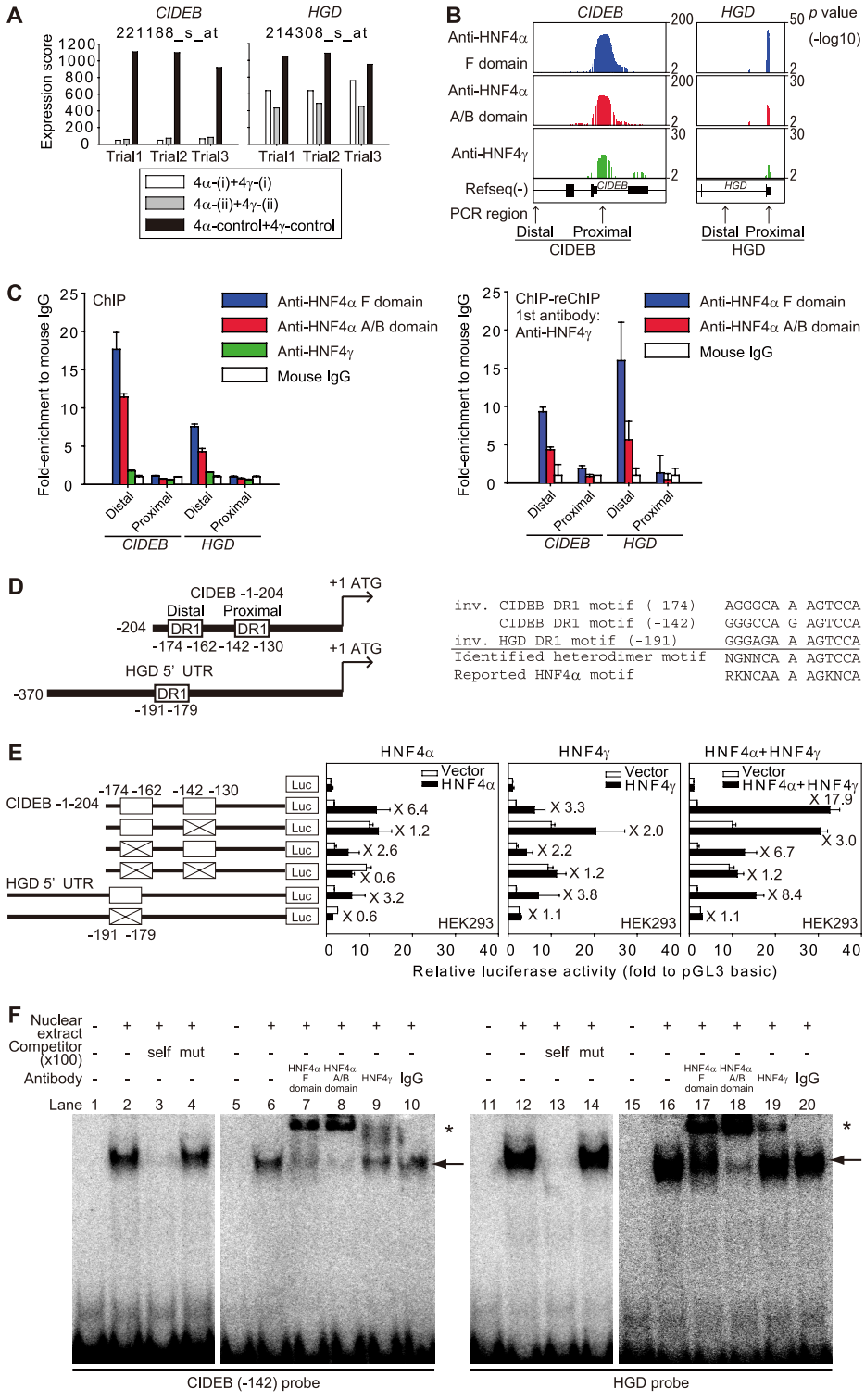

FIGURE 5. **The transcriptional activation of the *HGD* and *CIDEB* genes by HNF4α-HNF4γ heterodimerization through the same DR1 sites.** *A,* transcriptional down-regulation of *HGD* and *CIDEB* by siRNA-mediated HNF4α and -γ double knockdown in HepG2 cells. The ID of each probe is indicated *under* each gene name. *B,* the ChIP-seq analysis of HNF4α and HNF4γ overlap binding on the *CIDEB* and *HGD* promoter regions in HepG2 cells. The *arrows* denote the regions of the primer sets for ChIP-qPCR. *C,* ChIP-qPCR (*left*) and ChIP-reChIP-qPCR (*right*) analysis of HNF4α and HNF4γ overlap binding of the *CIDEB* short transcript and *HGD* promoter region in HepG2 cells. The details of the primer sets are provided under supplemental Table S1. *D, left*, schematic representation of the human *CIDEB* and *HGD* promoters, illustrating the DR1 motifs. *Right*, alignment of the two DR1 motifs in the human *CIDEB* and *HGD* promoters. The sequences of the DR1 motifs identified in the ChIP-seq study (Fig. 4*C*) (identified heterodimer motif) and the reported HNF4α binding motifs in HepG2 (Reported HNF4α motif) (72) are aligned. *E,* luciferase analysis of the HNF4α and HNF4γ cooperative transcriptional activity effect of the *CIDEB* and *HGD* genes on DR1 sequences. The relative luciferase activities of HNF4α (*left box*), HNF4γ (*center box*), and both HNF4α and HNF4γ (*right box*) are indicated. The *numbers above the bars* refer to the increases induced by each HNF4. *F,* EMSAs. The bands of DNA proteins in the HepG2 nuclear extract complex formations are indicated by the *arrow*. The bands of the complexes supershifted by the addition of each anti-HNF4 antibody are indicated by an *asterisk*. The oligonucleotide sequences used for probes and competitors are shown under supplemental Table S1. *HNF4α F domain*, anti-HNF4α F domain antibody H1415; *HNF4α A/B domain*, anti-HNF4α A/B domain antibody K9218; *HNF4γ*, anti-HNF4γ antibody B6502A.

transcriptional complexes under various stimulants, is highly useful for analyzing the complexity of the regulatory mechanisms of transcriptional regulation.

Acknowledgments—We thank Dr. Shogo Yamamoto for valuable advice on genome-wide analysis, and Dr. Kevin Boru of Pacific Edit for review of the manuscript. We also acknowledge Rie Fukuda, Yoko Chikaoka, Akashi Taguchi, and Aya Nakayama for excellent technical assistance.

REFERENCES

1. Kyrmizi, I., Hatzis, P., Katrakili, N., Tronche, F., Gonzalez, F. J., and Talianidis, I. (2006) *Genes Dev.* **20,** 2293–2305
2. Odom, D. T., Dowell, R. D., Jacobsen, E. S., Nekludova, L., Rolfe, P. A., Danford, T. W., Gifford, D. K., Fraenkel, E., Bell, G. I., and Young, R. A. (2006) *Mol. Syst. Biol.* **2,** 2006.0017
3. Watt, A. J., Garrison, W. D., and Duncan, S. A. (2003) *Hepatology* **37,** 1249–1253
4. Garrison, W. D., Battle, M. A., Yang, C., Kaestner, K. H., Sladek, F. M., and Duncan, S. A. (2006) *Gastroenterology* **130,** 1207–1220
5. Gupta, R. K., Gao, N., Gorski, R. K., White, P., Hardy, O. T., Rafiq, K., Brestelli, J. E., Chen, G., Stoeckert, C. J., Jr., and Kaestner, K. H. (2007) *Genes Dev.* **21,** 756–769
6. Hayhurst, G. P., Lee, Y. H., Lambert, G., Ward, J. M., and Gonzalez, F. J. (2001) *Mol. Cell. Biol.* **21,** 1393–1403
7. Stegmann, A., Hansen, M., Wang, Y., Larsen, J. B., Lund, L. R., Ritié, L., Nicholson, J. K., Quistorff, B., Simon-Assmann, P., Troelsen, J. T., and Olsen, J. (2006) *Physiol. Genomics* **27,** 141–155
8. Ellard, S., and Colclough, K. (2006) *Hum. Mutat.* **27,** 854–869
9. Navas, M. A., Munoz-Elias, E. J., Kim, J., Shih, D., and Stoffel, M. (1999) *Diabetes* **48,** 1459–1465
10. Hertz, R., Magenheim, J., Berman, I., and Bar-Tana, J. (1998) *Nature* **392,** 512–516
11. Wisely, G. B., Miller, A. B., Davis, R. G., Thornquest, A. D., Jr., Johnson, R., Spitzer, T., Sefler, A., Shearer, B., Moore, J. T., Miller, A. B., Willson, T. M., and Williams, S. P. (2002) *Structure* **10,** 1225–1234
12. Yuan, X., Ta, T. C., Lin, M., Evans, J. R., Dong, Y., Bolotin, E., Sherman, M. A., Forman, B. M., and Sladek, F. M. (2009) *PLoS One* **4,** e5609
13. Petrescu, A. D., Hertz, R., Bar-Tana, J., Schroeder, F., and Kier, A. B. (2005) *J. Biol. Chem.* **280,** 16714–16727
14. Odom, D. T., Zizlsperger, N., Gordon, D. B., Bell, G. W., Rinaldi, N. J., Murray, H. L., Volkert, T. L., Schreiber, J., Rolfe, P. A., Gifford, D. K., Fraenkel, E., Bell, G. I., and Young, R. A. (2004) *Science* **303,** 1378–1381
15. Guo, H., Gao, C., Mi, Z., Wai, P. Y., and Kuo, P. C. (2006) *Biochem. J.* **394,** 379–387
16. Ktistaki, E., Ktistakis, N. T., Papadogeorgaki, E., and Talianidis, I. (1995) *Proc. Natl. Acad. Sci. U.S.A.* **92,** 9876–9880
17. Viollet, B., Kahn, A., and Raymondjean, M. (1997) *Mol. Cell. Biol.* **17,** 4208–4219
18. Xu, Z., Tavares-Sanchez, O. L., Li, Q., Fernando, J., Rodriguez, C. M., Studer, E. J., Pandak, W. M., Hylemon, P. B., and Gil, G. (2007) *J. Biol. Chem.* **282,** 24607–24614
19. Kritis, A. A., Argyrokastritis, A., Moschonas, N. K., Power, S., Katrakili, N., Zannis, V. I., Cereghini, S., and Talianidis, I. (1996) *Gene* **173,** 275–280
20. Nakhei, H., Lingott, A., Lemm, I., and Ryffel, G. U. (1998) *Nucleic Acids Res.* **26,** 497–504
21. Hata, S., Tsukamoto, T., and Osumi, T. (1992) *Biochim. Biophys. Acta* **1131,** 211–213
22. Briançon, N., and Weiss, M. C. (2006) *EMBO J.* **25,** 1253–1262
23. Eeckhoute, J., Moerman, E., Bouckenooghe, T., Lukoviak, B., Pattou, F., Formstecher, P., Kerr-Conte, J., Vandewalle, B., and Laine, B. (2003) *Endocrinology* **144,** 1686–1694
24. Pascussi, J. M., Robert, A., Moreau, A., Ramos, J., Bioulac-Sage, P., Navarro, F., Blanc, P., Assenat, E., Maurel, P., and Vilarem, M. J. (2007) *Hepatology* **45,** 1146–1153
25. Sladek, F. M., Ruse, M. D., Jr., Nepomuceno, L., Huang, S. M., and Stallcup, M. R. (1999) *Mol. Cell. Biol.* **19,** 6509–6522
26. Perissi, V., and Rosenfeld, M. G. (2005) *Nat. Rev. Mol. Cell Biol.* **6,** 542–554
27. Rosenfeld, M. G., Lunyak, V. V., and Glass, C. K. (2006) *Genes Dev.* **20,** 1405–1428
28. Drewes, T., Senkel, S., Holewa, B., and Ryffel, G. U. (1996) *Mol. Cell. Biol.* **16,** 925–931
29. Ozeki, T., Takahashi, Y., Nakayama, K., Funayama, M., Nagashima, K., Kodama, T., and Kamataki, T. (2003) *Pharmacogenetics* **13,** 49–53
30. Plengvidhya, N., Antonellis, A., Wogan, L. T., Poleev, A., Borgschulze, M., Warram, J. H., Ryffel, G. U., Krolewski, A. S., and Doria, A. (1999) *Diabetes* **48,** 2099–2102
31. Archer, A., Sauvaget, D., Chauffeton, V., Bouchet, P. E., Chambaz, J., Pinçon-Raymond, M., Cardot, P., Ribeiro, A., and Lacasa, M. (2005) *Mol. Endocrinol.* **19,** 2320–2334
32. Ozeki, T., Takahashi, Y., Kume, T., Nakayama, K., Yokoi, T., Nunoya, K., Hara, A., and Kamataki, T. (2001) *Biochem. J.* **355,** 537–544
33. Ozeki, T., Takahashi, Y., Nakayama, K., and Kamataki, T. (2002) *Arch. Biochem. Biophys.* **405,** 185–190
34. Bogan, A. A., Dallas-Yang, Q., Ruse, M. D., Jr., Maeda, Y., Jiang, G., Nepomuceno, L., Scanlan, T. S., Cohen, F. E., and Sladek, F. M. (2000) *J. Mol. Biol.* **302,** 831–851
35. Sumi, K., Tanaka, T., Uchida, A., Magoori, K., Urashima, Y., Ohashi, R., Ohguchi, H., Okamura, M., Kudo, H., Daigo, K., Maejima, T., Kojima, N., Sakakibara, I., Jiang, S., Hasegawa, G., Kim, I., Osborne, T. F., Naito, M., Gonzalez, F. J., Hamakubo, T., Kodama, T., and Sakai, J. (2007) *Mol. Cell. Biol.* **27,** 4248–4260
36. Dignam, J. D., Lebovitz, R. M., and Roeder, R. G. (1983) *Nucleic Acids Res.* **11,** 1475–1489
37. Mathivanan, S., Ahmed, M., Ahn, N. G., Alexandre, H., Amanchy, R., Andrews, P. C., Bader, J. S., Balgley, B. M., Bantscheff, M., Bennett, K. L., Björling, E., Blagoev, B., Bose, R., Brahmachari, S. K., Burlingame, A. S., Bustelo, X. R., Cagney, G., Cantin, G. T., Cardasis, H. L., Celis, J. E., Chaerkady, R., Chu, F., Cole, P. A., Costello, C. E., Cotter, R. J., Crockett, D., DeLany, J. P., De Marzo, A. M., DeSouza, L. V., Deutsch, E. W., Dransfield, E., Drewes, G., Droit, A., Dunn, M. J., Elenitoba-Johnson, K., Ewing, R. M., Van Eyk, J., Faca, V., Falkner, J., Fang, X., Fenselau, C., Figeys, D., Gagné, P., Gelfi, C., Gevaert, K., Gimble, J. M., Gnad, F., Goel, R., Gromov, P., Hanash, S. M., Hancock, W. S., Harsha, H. C., Hart, G., Hays, F., He, F., Hebbar, P., Helsens, K., Hermeking, H., Hide, W., Hjernø, K., Hochstrasser, D. F., Hofmann, O., Horn, D. M., Hruban, R. H., Ibarrola, N., James, P., Jensen, O. N., Jensen, P. H., Jung, P., Kandasamy, K., Kheterpal, I., Kikuno, R. F., Korf, U., Körner, R., Kuster, B., Kwon, M. S., Lee, H. J., Lee, Y. J., Lefevre, M., Lehvaslaiho, M., Lescuyer, P., Levander, F., Lim, M. S., Löbke, C., Loo, J. A., Mann, M., Martens, L., Martinez-Heredia, J., McComb, M., McRedmond, J., Mehrle, A., Menon, R., Miller, C. A., Mischak, H., Mohan, S. S., Mohmood, R., Molina, H., Moran, M. F., Morgan, J. D., Moritz, R., Morzel, M., Muddiman, D. C., Nalli, A., Navarro, J. D., Neubert, T. A., Ohara, O., Oliva, R., Omenn, G. S., Oyama, M., Paik, Y. K., Pennington, K., Pepperkok, R., Periaswamy, B., Petricoin, E. F., Poirier, G. G., Prasad, T. S., Purvine, S. O., Rahiman, B. A., Ramachandran, P., Ramachandra, Y. L., Rice, R. H., Rick, J., Ronnholm, R. H., Salonen, J., Sanchez, J. C., Sayd, T., Seshi, B., Shankari, K., Sheng, S. J., Shetty, V., Shivakumar, K., Simpson, R. J., Sirdeshmukh, R., Siu, K. W., Smith, J. C., Smith, R. D., States, D. J., Sugano, S., Sullivan, M., Superti-Furga, G., Takatalo, M., Thongboonkerd, V., Trinidad, J. C., Uhlen, M., Vandekerckhove, J., Vasilescu, J., Veenstra, T. D., Vidal-Taboada, J. M., Vihinen, M., Wait, R., Wang, X., Wiemann, S., Wu, B., Xu, T., Yates, J. R., Zhong, J., Zhou, M., Zhu, Y., Zurbig, P., and Pandey, A. (2008) *Nat. Biotechnol.* **26,** 164–167
38. Tanaka, T., Jiang, S., Hotta, H., Takano, K., Iwanari, H., Sumi, K., Daigo, K., Ohashi, R., Sugai, M., Ikegame, C., Umezu, H., Hirayama, Y., Midorikawa, Y., Hippo, Y., Watanabe, A., Uchiyama, Y., Hasegawa, G., Reid, P., Aburatani, H., Hamakubo, T., Sakai, J., Naito, M., and Kodama, T. (2006) *J. Pathol.* **208,** 662–672
39. Sakamoto, A., Kawasaki, T., Kazawa, T., Ohashi, R., Jiang, S., Maejima,

T., Tanaka, T., Iwanari, H., Hamakubo, T., Sakai, J., Kodama, T., and Naito, M. (2007) *J. Histochem. Cytochem.* **55,** 641–649
40. Wakabayashi, K., Okamura, M., Tsutsumi, S., Nishikawa, N. S., Tanaka, T., Sakakibara, I., Kitakami, J., Ihara, S., Hashimoto, Y., Hamakubo, T., Kodama, T., Aburatani, H., and Sakai, J. (2009) *Mol. Cell. Biol.* **29,** 3544–3555
41. Wolfertstetter, F., Frech, K., Herrmann, G., and Werner, T. (1996) *Comput. Appl. Biosci.* **12,** 71–80
42. Cartharius, K., Frech, K., Grote, K., Klocke, B., Haltmeier, M., Klingenhoff, A., Frisch, M., Bayerlein, M., and Werner, T. (2005) *Bioinformatics* **21,** 2933–2942
43. Song, H., Suehiro, J., Kanki, Y., Kawai, Y., Inoue, K., Daida, H., Yano, K., Ohhashi, T., Oettgen, P., Aird, W. C., Kodama, T., and Minami, T. (2009) *J. Biol. Chem.* **284,** 29109–29124
44. America, A. H., and Cordewener, J. H. (2008) *Proteomics* **8,** 731–749
45. Silva, J. C., Gorenstein, M. V., Li, G. Z., Vissers, J. P., and Geromanos, S. J. (2006) *Mol. Cell. Proteomics* **5,** 144–156
46. Ikura, T., Ogryzko, V. V., Grigoriev, M., Groisman, R., Wang, J., Horikoshi, M., Scully, R., Qin, J., and Nakatani, Y. (2000) *Cell* **102,** 463–473
47. Martinez, E., Palhan, V. B., Tjernberg, A., Lymar, E. S., Gamper, A. M., Kundu, T. K., Chait, B. T., and Roeder, R. G. (2001) *Mol. Cell. Biol.* **21,** 6782–6795
48. Will, C. L., Urlaub, H., Achsel, T., Gentzel, M., Wilm, M., and Lührmann, R. (2002) *EMBO J.* **21,** 4978–4988
49. Zhang, C., Dowd, D. R., Staal, A., Gu, C., Lian, J. B., van Wijnen, A. J., Stein, G. S., and MacDonald, P. N. (2003) *J. Biol. Chem.* **278,** 35325–35336
50. Kitagawa, H., Fujiki, R., Yoshimura, K., Mezaki, Y., Uematsu, Y., Matsui, D., Ogawa, S., Unno, K., Okubo, M., Tokita, A., Nakagawa, T., Ito, T., Ishimi, Y., Nagasawa, H., Matsumoto, T., Yanagisawa, J., and Kato, S. (2003) *Cell* **113,** 905–917
51. Denslow, S. A., and Wade, P. A. (2007) *Oncogene* **26,** 5433–5438
52. Wang, Z., Zang, C., Cui, K., Schones, D. E., Barski, A., Peng, W., and Zhao, K. (2009) *Cell* **138,** 1019–1031
53. Da, L., Li, D., Yokoyama, K. K., Li, T., and Zhao, M. (2006) *Biochem. J.* **393,** 779–788
54. Li, J. Z., Ye, J., Xue, B., Qi, J., Zhang, J., Zhou, Z., Li, Q., Wen, Z., and Li, P. (2007) *Diabetes* **56,** 2523–2532
55. Fernández-Cañón, J. M., Granadino, B., Beltrán-Valero de Bernabé, D., Renedo, M., Fernández-Ruiz, E., Peñalva, M. A., and Rodríguez de Córdoba, S. (1996) *Nat. Genet.* **14,** 19–24
56. Gonzalez, F. J. (2008) *Drug Metab. Pharmacokinet.* **23,** 2–7
57. Takegoshi, S., Jiang, S., Ohashi, R., Savchenko, A. S., Iwanari, H., Tanaka, T., Hasegawa, G., Hamakubo, T., Kodama, T., and Naito, M. (2009) *Pathol. Int.* **59,** 61–72
58. Mayeur, G. L., Kung, W. J., Martinez, A., Izumiya, C., Chen, D. J., and Kung, H. J. (2005) *J. Biol. Chem.* **280,** 10827–10833
59. Nock, A., Ascano, J. M., Jones, T., Barrero, M. J., Sugiyama, N., Tomita, M., Ishihama, Y., and Malik, S. (2009) *J. Biol. Chem.* **284,** 19915–19926
60. Zhao, Y., Lang, G., Ito, S., Bonnet, J., Metzger, E., Sawatsubashi, S., Suzuki, E., Le Guezennec, X., Stunnenberg, H. G., Krasnov, A., Georgieva, S. G., Schüle, R., Takeyama, K., Kato, S., Tora, L., and Devys, D. (2008) *Mol. Cell* **29,** 92–101
61. Brann, D. W., Zhang, Q. G., Wang, R. M., Mahesh, V. B., and Vadlamudi, R. K. (2008) *Mol. Cell. Endocrinol.* **290,** 2–7
62. Wagner, N., and Krohne, G. (2007) *Int. Rev. Cytol.* **261,** 1–46
63. Christensen, J., Agger, K., Cloos, P. A., Pasini, D., Rose, S., Sennels, L., Rappsilber, J., Hansen, K. H., Salcini, A. E., and Helin, K. (2007) *Cell* **128,** 1063–1076
64. Shi, Y., Lan, F., Matson, C., Mulligan, P., Whetstine, J. R., Cole, P. A., Casero, R. A., and Shi, Y. (2004) *Cell* **119,** 941–953
65. Lee, J. W., Choi, H. S., Gyuris, J., Brent, R., and Moore, D. D. (1995) *Mol. Endocrinol.* **9,** 243–254
66. Chan, S. W., and Hong, W. (2001) *J. Biol. Chem.* **276,** 28402–28412
67. Wang, Y., Zhang, H., Chen, Y., Sun, Y., Yang, F., Yu, W., Liang, J., Sun, L., Yang, X., Shi, L., Li, R., Li, Y., Zhang, Y., Li, Q., Yi, X., and Shang, Y. (2009) *Cell* **138,** 660–672
68. Giovannone, B., Lee, E., Laviola, L., Giorgino, F., Cleveland, K. A., and Smith, R. J. (2003) *J. Biol. Chem.* **278,** 31564–31573
69. Kulkarni, R. N., and Kahn, C. R. (2004) *Science* **303,** 1311–1312
70. Araya, N., Hirota, K., Shimamoto, Y., Miyagishi, M., Yoshida, E., Ishida, J., Kaneko, S., Kaneko, M., Nakajima, T., and Fukamizu, A. (2003) *J. Biol. Chem.* **278,** 5427–5432
71. Kim, H. J., Lee, S. K., Na, S. Y., Choi, H. S., and Lee, J. W. (1998) *Mol. Endocrinol.* **12,** 1038–1047
72. Rada-Iglesias, A., Wallerman, O., Koch, C., Ameur, A., Enroth, S., Clelland, G., Wester, K., Wilcox, S., Dovey, O. M., Ellis, P. D., Wraight, V. L., James, K., Andrews, R., Langford, C., Dhami, P., Carter, N., Vetrie, D., Pontén, F., Komorowski, J., Dunham, I., and Wadelius, C. (2005) *Hum. Mol. Genet.* **14,** 3435–3447
73. Araya, N., Hiraga, H., Kako, K., Arao, Y., Kato, S., and Fukamizu, A. (2005) *Biochem. Biophys. Res. Commun.* **329,** 653–660